Journal of Materials Chemistry C

PAPER

View Article Online
View Journal | View Issue





Cite this: J. Mater. Chem. C, 2017, 5, 3561

# Novel bonding patterns and optoelectronic properties of the two-dimensional $Si_xC_y$ monolayers†

Dong Fan, [a] Shaohua Lu,*[a] Yundong Guo[b] and Xiaojun Hu *[a]

Received 15th December 2016,
Accepted 27th February 2017

DOI: 10.1039/c6tc05415c

rsc.li/materials-c

The search for new two-dimensional (2D) materials with novel optical and electronic properties is always desirable for material development. Herein, we report a comprehensive theoretical prediction of 2D SiC compounds with different stoichiometries from C-rich to Si-rich. In addition to the previously known hexagonal SiC sheet, we identified two types of hitherto-unknown structural motifs with distinctive bonding features. The first type of 2D SiC monolayer, including t-SiC and t-$Si_2C$ sheet, can be described by tetragonal lattice. Among them, t-SiC monolayer sheet is featured by each carbon atom binding with four neighboring silicon atoms in almost the same plane, constituting a quasi-planar four-coordinated rectangular moiety. More interestingly, our calculations demonstrate that this structure exhibits a strain-dependent insulator–semimetal transition, suggesting promising applications in strain-dependent optoelectronic sensors. The second type of 2D SiC sheet is featured by silagraphyne with acetylenic linkages (–C≡C–). Silagraphyne shows both high pore sizes and Poisson's ratio. These properties make it a potentially important material for applications in separation membranes and catalysis. Moreover, one of the proposed structures, γ-silagraphyne, is a direct-band-gap semiconductor with a bandgap of 0.89 eV, which has a strong absorption peak in the visible-light region, giving a promising application in ultra-thin transistors, optical sensor devices and solar cell devices.

## 1. Introduction

Since the demonstration of the first isolated graphene sheet in 2004, 2D atomic crystals have received much attention. For graphene, due to its numerous extraordinary properties, it has potential applications in a wide range of areas. However, the pristine graphene is a gapless semi-metal, which means that it is difficult to control the number of carriers. This dramatically limits its applications in the field effect transistor, photovoltaic cell, *etc.* Thus, the subject of finding new 2D materials other than graphene is one of the most active fields of current material research. This research includes graphyne,[1] single-layer hexagonal boron nitride (h-BN),[2,3] transition metal oxides or chalcogenides,[4,5] phosphorene,[6] as well as group IV–VI and III–V layered crystals.[7] Specifically, in addition to graphene and graphyne, a strong research topic in group-IV 2D elemental monolayers has sprung up in recent years.[8–10] However, these group-IV 2D elemental derivatives show the properties of Dirac fermion behavior without spin–orbit coupling, which creates a set of challenges for application in conventional electronic devices due to the lack of band gap at the Fermi level.

2D SiC has recently emerged as a promising material with tunable band gaps for potential applications in optoelectronics and electronics.[11] Particularly inspired by the successful syntheses of the graphene-like hexagonal SiC sheet in experiments,[12] a few carbon-rich SiC monolayers, such as *para*-$SiC_3$,[13] g-$SiC_2$,[14] and pt-$SiC_2$,[15] were predicted at one particular stoichiometry. Among all of these new structures, the g-$SiC_2$ sheet, with a direct band gap of 1.09 eV is a nearly ideal material for flexible optoelectronic devices. Recently, using first-principle calculations coupled with the cluster expansion method, Shi *et al.* reported a structural search on SiC sheets with different stoichiometry.[16] However, their structure search is limited to a graphene-like hexagonal lattice. Therefore, in order to further explore the configuration space and unique properties of SiC sheets, a global structure search with both variable lattice type and stoichiometry is required.

In this study, we report a range of low-energy $Si_xC_y$ monolayers with distinguished bonding patterns and electronic properties using an unbiased particle swarm optimization (PSO) structure search algorithm.[17] Flat hexagonal lattices have

[a] College of Materials Science and Engineering, Zhejiang University of Technology, Hangzhou 310014, China. E-mail: lsh@zjut.edu.cn, huxj@zjut.edu.cn; Fax: +86-571-88871522; Tel: +86-571-88871522
[b] School of Engineering and Technology, Neijiang Normal University, Neijiang, 641000, China

† Electronic supplementary information (ESI) available. See DOI: 10.1039/c6tc05415c

been successfully predicted as the low-energy structures for previously reported g-$SiC_2$, SiC and several other $Si_xC_y$ monolayers in this study. Based on comprehensive analysis and simulations, we found 2D tetragonal silagraphene named t-SiC and t-$Si_2C$ sheets to have both thermodynamic and mechanical stability. The t-SiC exists as a buckled tetragonal atomic arrangement formed by strong $C_{2p}$–$Si_{3p}$ bonding with an out-of-plane electron delocalization. More importantly, a phase transition from direct band gap semiconductor to semi-metal is observed when biaxial tensile strain is exerted on the t-SiC monolayer, suggesting promising applications in strain-dependent optoelectronic sensors. Moreover, six different silagraphyne sheets with higher pore sizes and Poisson's ratio were found, making them potential candidates for separation membranes and catalytic materials. Particularly for γ-silagraphyne, it exhibits direct band gap and prominent optical absorption in the visible-light spectrum, indicating to be a desirable material in microelectronics, solar cell materials and nanoscale optical sensor devices.

## 2. Computational methods

Candidate structures were obtained using a global structural optimization method, as implemented in CALYPSO code.[17] It has been successfully applied to various crystal surfaces and low dimensional materials.[18–20] A structure search was performed with the concentration of carbon ranging from 0.167 to 0.833. The subsequent structural relaxation and total energy calculations were carried out using the density functional theory (DFT) in applying general gradient approximation (GGA) in the Perdew–Burke–Ernzerhof (PBE)[21] parameterization for exchange correlation potential, as implemented in the Vienna *ab initio* simulation package (VASP).[22] The plane wave cut off energy was set to 650 eV. The convergence criterion of self-consistent calculations for ionic relaxations was $10^{-5}$ eV between two consecutive steps, and the atomic positions and unit cells were optimized until the atomic forces were less than 0.01 eV $Å^{-1}$ without any symmetry constraints. A slab model containing a 20 Å vacuum region in the normal direction was selected to simulate isolated 2D materials. The *z*-axis was fixed during structure relaxation. Heyd–Scuseria–Ernzerhof (HSE06) functional was used to calculate band structures of selected configurations.[23] In order to study the dynamical stability of the proposed structures, we performed phonon calculations and *ab initio* molecular dynamics (AIMD) simulations. Phonon calculations were conducted by the density functional perturbation theory (DFPT) method using the PHONOPY code.[24] AIMD simulations were carried out in the *NVT* ensemble with a time step of 1 fs for a total time of 5 ps. We collected structures with the lowest energies at each stoichiometric composition and calculated the formation energy ($E_f$) to evaluate the relative stabilities of the predicted 2D SiC compounds, which are defined as follows:

$$E_f = (E_{si_xC_y} - x\mu_{Si} - y\mu_C)/(x + y)$$

where $E_f$ denotes the formation energy of the corresponding 2D SiC compounds, $E_{Si}$, $E_C$ and $E_{si_xC_y}$ are the total energy of a single Si atom in silicene, a single C atom in graphene, and the 2D $Si_xC_y$ compound, respectively.

## 3. Results and discussions

Fig. 1 shows the schematic of the calculated formation energies of $Si_xC_y$ sheets under conditions from C-rich to Si-rich. Previously known sheets, such as hexagonal SiC, *para*-$SiC_3$, g-$SiC_2$, and pt-$SiC_2$ have been successfully reproduced in this study, and our calculated formation energies are consistent with previous results. In addition, two types of hitherto unknown structure motifs are revealed in the global structure search. The predicted low-energy structures of several allotropes with unique bonding patterns and the corresponding lattice parameters are listed in Table S1 (ESI†). All 2D compounds with novel bonding geometries are predicted and plotted in Fig. 2, Fig. S1 and S2 (ESI†). Moreover, kinetic stability of these 2D sheets is verified by both phonon spectrum calculations and AIMD simulations. Next, we perform a systematic analysis of the chemical bonding and mechanical and electronic properties on the newly found structures.

### 3.1 Atomic configurations and bonding features

Fig. 2a displays the geometric configuration of the t-SiC monolayer. Its rectangular lattice constants are $a$ = 3.67 Å and $b$ = 3.21 Å, with a thickness $c$ = 1.42 Å. One unit-cell of t-SiC consists of 2 C atoms and 2 Si atoms, respectively. Specifically, all the atoms in the supercell bond to four neighboring atoms. Usually, just like graphene, the majority of 2D sheets have three-fold coordinated bonding moieties. All C and Si atoms in the t-SiC sheet are quasi-planar tetracoordinated atoms. To the best of our knowledge, this is the first time that a study on pure tetracoordinated carbon

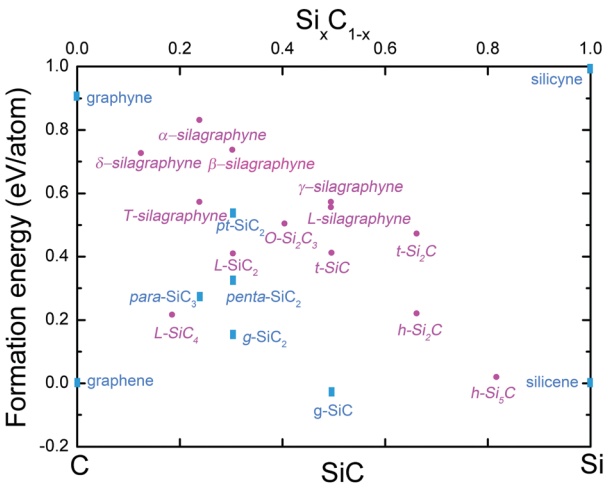


Fig. 1 Schematic of the calculated formation energies ($E_f$) of various compounds with respect to elemental decomposition into graphene and silicene. Herein, we chose the generally accepted reference state (graphene and silicene in 2D space) to evaluate the thermodynamic stability of 2D $Si_xC_{1-x}$ sheets. When $x$ = 0 ($x$ = 1), according to the definition of the $E_f$, the calculated $E_f$ for graphene (silicene) is 0. For comparison, the calculated formation energy values of previously known 2D compounds, *i.e.*, *para*-$SiC_3$,[13] g-$SiC_2$,[14] pt-$SiC_2$[15] and penta-$SiC_2$,[41] are also plotted.

 

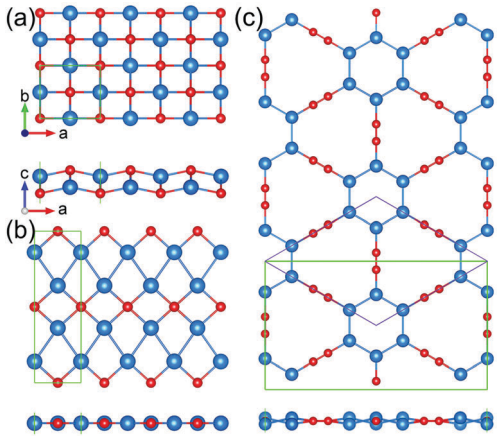


Fig. 2 Top (upper) and side (lower) views of the structure of (a) t-SiC, (b) t-$Si_2C$ and (c) γ-silagraphyne monolayer. The blue and red balls represent Si and C atoms, respectively. The rhombohedra (violet) and rectangular (green) unit cells are presented.

atoms in 2D covalent materials has been reported. The stabilizing mechanisms and bonding characteristics are disclosed by analyzing the deformation electron density data, which is defined as the total electronic density of the 2D SiC system excluding the electronic densities of isolated Si and C atoms.

The stability of the new structures can be illustrated by examining their deformation electron density, which reveals the electron transfer from the Si to C atom as shown in Fig. S3 (ESI†). The transferred electrons mainly originated from the Si atoms of t-SiC. To minimize the Coulomb repulsion, C atoms buckle out of the plane to increase the distance between the two neighboring Si atoms. As a result, the C–Si bond length in the buckled structure is 1.92 and 1.87 Å along the *a* and *b* directions, respectively. In order to gain deeper insight into the stability of the bonding, we plot the electron localization function (ELF) and the orbital-projected density of states (DOS). An isosurface of ELF for t-SiC is illustrated in Fig. S4 (ESI†), with an isovalue of 0.80 a.u., indicating the formation of strong C–Si σ bonds. It is found that the electrons are mainly localized on the C–Si bonds, and the dumb-bell shape of the C-$p_z$ orbitals has a large deformation spreading along the bonds, which is crucial to stabilizing these quasi-planar tetracoordinate atoms since it not only weakens the activity of atomic Si and C to form out-of-plane bonds, but also strengthens the in-plane C–Si bonds. Moreover, as shown in Fig. S5 (ESI†), the Si-3p and C-2p orbitals are mainly distributed in the energy range of 0.0–2.0 eV below the valence band maximum, suggesting a strong hybridization between them and a covalent bonding feature with both Si and C atoms. Thus, localization of the electrons in the C-$p_z$ orbital and the Si-3p and C-2p hybridization explain the stability of t-SiC.

Another structure (labeled as t-$Si_2C$) with tetragonal lattice is also revealed. As shown in Fig. 2b, the t-$Si_2C$ monolayer forms an exactly planar structure and the optimized lattice constants for the t-$Si_2C$ monolayer are $a$ = 2.79 Å and $b$ = 9.09 Å. Deformation charge density also shows the electron transfer from Si atoms to C atoms in the t-$Si_2C$ monolayer. Its ELF isosurfaces exhibit two domains: one is the distribution around the centered four C–Si bonds symmetrically and the other is the Si–Si dimer rows, whereas the bonding between adjacent Si atoms is weak compared with C–Si σ bonds. However, different from t-SiC, some electrons are extracted from the $3p_z$ orbital of the Si atoms and delocalized over four C–Si bonds in the same plane, suggesting the covalent character of C–Si bonds. Hence, the covalent C–Si bonds and the existance of Si–Si bonds play a crucial role in stabilization of the crystal structure, giving rise to a nearly planar tetracoordinate carbon network.

In addition to tetragonal silagraphene, we also demonstrate a new 2D SiC monolayer with acetylenic linkages (–C≡C–), namely, silagraphyne. Fig. 2 and Fig. S1 (ESI†) display three 2D SiC compounds, one being silagraphyne, which contains acetylenic linkages that are more stable than those of graphyne with respect to their formation energies. It is worth noting that the shortest distances between sp-carbon atoms are 1.24 and 1.23 Å of α(β)-silagraphyne and γ-silagraphyne, respectively. This indicates that the localization of electron density is in the binding regions. As demonstrated in Fig. S1 and S2 (ESI†), all the structures of silagraphyne, except for ʟ- and γ-silagraphyne with a buckling of 0.65 and 0.48 Å, are purely planar. It is clearly seen that the acetylenic linkages generate pores, which are much larger than those in graphene and graphyne.[25] According to our calculations, α-, β- and γ-silagraphyne have the inverse of the specific surface area of 0.362, 0.432 and 0.537 mg $m^{-2}$, respectively. This size of the pore is a crucial aspect for the material's use in desalination of sea water,[26] photocatalyst,[27] lithium-ion battery and energy storage.[28] These materials have high porosity and high specific surface area compared to graphyne (*i.e.*, 0.379 mg $m^{-2}$ for α-graphyne, 0.461 mg $m^{-2}$ for β-graphyne and 0.582 mg $m^{-2}$ for γ-graphyne).[25] The calculated ELF maps of silagraphyne monolayers are demonstrated in Fig. S6 (ESI†). It is clearly seen that all of the ELFs of C–C and C–Si bonds are localized at the bond center, similar to the ELF maps in the t-SiC monolayer.

### 3.2 Energetic stability

The stability of the 2D $Si_xC_y$ sheet can first be understood by calculating its formation and cohesive energies, as shown in Fig. 1 and Table S1 (ESI†). The results show that newly predicted t-SiC is higher in energy than graphene by 0.39 eV per atom, but lower than the previously reported pt-$SiC_2$ by 0.19 eV per atom. Simultaneously, the cohesive energies of t-SiC and t-$Si_2C$ are 5.55 and 4.85 eV per atom, respectively, which are larger than that of silicene (3.93 eV per atom) and lower than that of graphene (7.94 eV per atom). Thus, it is proven that a 2D tetragonal SiC monolayer has higher structural stability and stronger binding energy compared with silicene. Clearly, the silagraphyne monolayers are metastable, while they all have lower formation energies with respect to graphene and silicene. In particular, we also note that silagraphyne monolayers are energetically preferable over the experimentally confirmed graphdiyne films.[29] This implies that the newly found silagraphyne sheets might be synthesized in the experiment. Moreover, we calculated the cohesive energy to evaluate the stability of the proposed

silagraphyne structures. As shown in Table S1 (ESI†), the cohesive energies of silagraphyne monolayers range from 4.50 to 6.55 eV per atom, which is significantly lower than that of graphene, but still higher than that of silicene, attesting that the silagraphyne sheets are energetically stable.

### 3.3 Kinetic stability

To examine the dynamic stability of the proposed structures, the phonon dispersion spectra and phonon density of states (Ph DOS) were calculated using the DFPT method along the high-symmetry lines, as shown in Fig. 3 and Fig. S7 (ESI†). It is observed that there is no imaginary phonon frequency in the entire Brillouin zone, confirming that tetragonal silagraphene sheets are dynamically stable. For the t-SiC and t-$Si_2C$ monolayer, we note that the highest frequency reaches up to 735 and 713 $cm^{-1}$, respectively, which is slightly higher than that of silicene (580 $cm^{-1}$)[9] and the $MoS_2$ monolayer (473 $cm^{-1}$),[30] indicating robust C–Si bonds in these 2D systems. Analysis of partial Ph DOS reveals that the highest frequency of t-SiC mainly originates from C atoms.

Fig. 3c shows that the highest in-plane optical branches of t-SiC rise to 735 $cm^{-1}$, corresponding to the relative stretching vibration between Si and C atoms. The phonon dispersion curves of t-$Si_2C$ indicate the presence of a phonon gap and have the separation of acoustic and optical branches with the maximum vibrational frequency at ~368 $cm^{-1}$. Detailed analysis of the Ph DOS and phonon mode reveals that the lower acoustic modes are associated with the constituent of Si atoms, while the high frequency vibrational modes are attributed to the in-plane stretching modes of the systems (as seen in Fig. 3d).

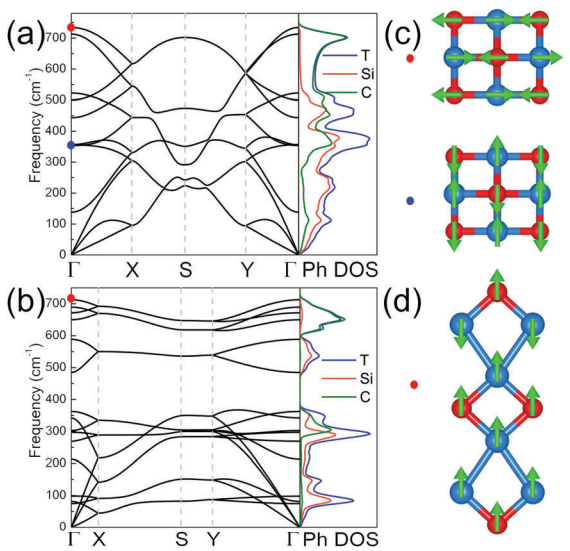


Fig. 3 Phonon band dispersions (left panel) and partial Ph DOS (right panel) of (a) t-SiC and (b) t-$Si_2C$ monolayer are calculated by the DFPT method. (c and d) Corresponding phonon vibration modes at 735 $cm^{-1}$ (354 $cm^{-1}$) and 713 $cm^{-1}$. As expected, the highest vibration frequency of phonons for 2D SiC systems is in the range of graphene (≈1581 $cm^{-1}$), and silicene (≈580 $cm^{-1}$). *Γ* (0, 0, 0), *X* (1/2, 0, 0), *S* (1/2, 1/2, 0) and *Y* (0, 1/2, 0) refer to special points in the first Brillouin zone of reciprocal space. There is no imaginary frequency in the whole path.

To further understand the stability of these unique structures at ambient conditions, we performed AIMD simulations within the canonical *NVT* ensemble at 1000 K for 5 ps with a time step of 1 fs. Total energy development of simulation time and snapshots taken at the end of each time is shown in Fig. S8–S10 (ESI†). During the final *NVT* simulation, t-SiC and t-$Si_2C$ sheets are stable up to a temperature of 800 K, while other silagraphene and silagraphyne can maintain the structural integrity at 1000 K (Fig. S9 and S10, ESI†). The above-mentioned results reveal that these 2D SiC monolayers exhibit a high thermal stability.

### 3.4 Mechanical properties

For a mechanically stable 2D material, the elastic constants need to fulfill the following requirements: $C_{11}C_{22} - C_{12}C_{21} > 0$ and $C_{66} > 0$.[31] For silagraphene, the calculated elastic constants satisfy this formula, and the calculated $C_{66}$ is positive (Table S2, ESI†), indicating that all the proposed silagraphene sheets are mechanically stable. The in-plane stiffness modulus can be derived from the elastic constants by $E = (C_{11}C_{22} - C_{12}C_{21})/C_{11}$. Tetragonal silagraphene sheets present elastic in-plane stiffness with 119 and 169 GPa·nm along the *b* direction for t-SiC and t-$Si_2C$, respectively, which are more than double that of silicene. The calculated elastic constants of six silagraphyne monolayers also satisfy the mechanical stability criteria, indicating that the 2D silagraphyne monolayers are mechanically stable (Table S3, ESI†). Interestingly, the calculated in-plane stiffness values for three types of silagraphyne going from α-silagraphyne, to β- and γ-silagraphyne are 17.00, 26.33 and 47.55 GPa nm, respectively. The in-plane stiffness increases with decreasing specific surface area and is significantly lower than that of graphyne. Thus, these 2D sheets inserting acetylenic linkages are much softer than graphyne and graphene due to the lower planar packing densities of these structures with respect to the graphene. Similar to graphyne, α-, β- and γ-silagraphyne have Poisson's ratios between 0.5 and 1, suggesting a higher structural deformation along the perpendicular direction to the plane.[25]

### 3.5 Electronic structure

Fig. 4 shows the band structures (calculated *via* the HSE functional) of t-SiC and t-$Si_2C$ structures. As presented in Fig. 4a, t-SiC is a direct band gap semiconductor with a band gap of 1.84 eV (0.85 eV at the PBE level) at the *Γ* point. Its conduction band minimum (CBM) is contributed by the Si-3s (σ) orbitals, while the valence band maximum (VBM) is contributed by Si-3p (π) and C-2p (π) orbitals (Fig. S5, ESI†). However, different from t-SiC, our band structure calculations show that t-$Si_2C$ is metallic with a finite density of states at the Fermi energy. Fig. 4c(e) and d(f) indicate the highest occupied orbital (HOMO) and the lowest unoccupied orbital (LUMO) at the *Γ* point, respectively. It is interesting to note that, for t-$Si_2C$, the HOMO clearly shows the strong bonding between two Si atoms, while LUMO is mainly distributed around the Si atoms. Therefore, the $3p_z$ electrons on the Si atoms and the $2p_z$ orbitals

 

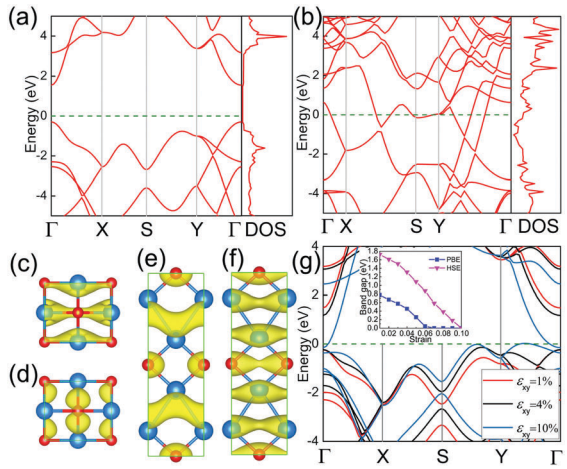


Fig. 4 Electronic band structure and DOS of (a) t-SiC and (b) t-$Si_2C$ structures are calculated using the HSE06 functional. Band-decomposed charge density distributions are illustrated in c to f. (c) The highest occupied electronic state and (d) the lowest unoccupied electronic state of t-SiC at the $\Gamma$ point. (e) The highest occupied electronic state and (f) the lowest unoccupied electronic state of t-$Si_2C$ at the $\Gamma$ point. The Fermi level is set to zero and marked by the dashed lines. (g) Band structure of t-SiC with different biaxial strains. Inset shows the band gap of the monolayer as a function of biaxial strains (calculated by PBE and HSE06 functionals).

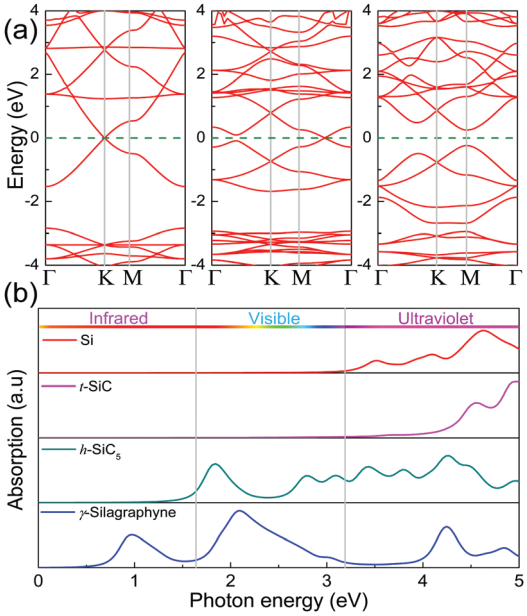


Fig. 5 (a) Calculated band structure of α-silagraphyne (left), β-silagraphyne (middle), and γ-silagraphyne (right) monolayers. The Fermi level is set to zero and marked by dashed lines. (b) Optical absorption coefficient of the proposed structures; silicon data is presented for comparison (calculated by HSE06 functional).

on the C atoms occupy near the Fermi level, which results in the appearance of the metallic property in the t-$Si_2C$ sheet. Fig. S11 (ESI†) also shows the phonon dispersion for the t-SiC sheet when biaxial strain is applied, for strain values of 1%, 9% and −9%. There is no imaginary phonon mode in phonon dispersion, and hence its strained monolayer is also stable.

Subsequently, for the t-SiC sheet, we calculate the HSE band structure at different biaxial strain (Fig. 4g). Notably, we find that the band structure can be transformed from direct band gap to semimetal at a relatively suitable biaxial strain (10%). To further explore the origin of this transformation, we calculated the deformation charge density and orbital-resolved band structures of no-strained and 10% strained t-SiC sheet (Fig. S12 and S13, ESI†). The results suggest that the Si atoms of the 10% strained t-SiC have less charge transferred to the C atoms, indicating that the electrons in the Si atoms are more delocalized. ELF maps further confirm that the presence of metallicity of 10% strained t-SiC is intimately related with the delocalized states. On the other side, the direct band gap persists under a tensile strain from 1% to 4% and the band gap decreases from 1.72 to 1.31 eV. According to the Shockley–Queisser limit,[32] for single-gap photovoltaic devices with the band gap of 1.34 eV, a maximum photoelectric conversion efficiency of 33.7% can be achieved. Thus, the direct band structure of a small strained monolayer supplies an advantage for application in photoelectric devices.

Fig. 5a and Fig. S14 (ESI†) demonstrate the electronic band structures of a few selected silagraphyne monolayers calculated with the PBE functional. It is observed that α-silagraphyne and β-silagraphyne show the presence of Dirac points at the Fermi level, but they show a different number and location of Dirac points. α-Silagraphyne has Dirac points located at *K* high symmetry points, while β-silagraphyne has Dirac points in the *Γ*–*M* direction. These interesting results are similar to the electronic structure of graphyne. However, γ-silagraphyne and T-silagraphyne show direct band gaps, where the CBM and VBM are located at the *M* and *Γ* points in the Brillouin zone, respectively. Using the HSE functional, we note that γ-silagraphyne and T-silagraphyne have the band gap of 0.89 and 2.02 eV, respectively, while δ-silagraphyne and L-silagraphyne show semimetal properties.

### 3.6 Optical properties and possible fabrication scheme

Band gap plays a fundamental role in semiconductor materials, due to the strong dependence of band gap and solar cells energy conversion efficiency.[32] The characteristics of the moderate direct band gap for 2D SiC monolayers make them promising solar-cell absorption materials. Thus, optical absorption spectra of predicted low energy structures were calculated at the HSE06 level. For comparison, calculations were also carried out for silicon. Our results for the silicon curves are in accordance with previous calculations.[33] Fig. 5b shows the optical absorption spectra. According to the spectral range, we separated the absorption spectrum into three parts, namely the infrared, visible, and ultraviolet regions. Analogous to silicon, due to the large direct band gap, the t-SiC monolayer can absorb photons mostly in the ultraviolet range. Surprisingly, γ-silagraphyne can absorb sunlight at lower energies than that of the t-SiC sheet, implying that this structure can capture more sunlight and make more efficient use of solar energy compared to that of silicon.

The aforementioned results suggest that tetragonal silagraphene and silagraphyne are very promising candidates for application in future optoelectronic nanodevices due to their unique structural

and electronic properties. Thus, it is desirable to synthesize these new monolayers experimentally. Compared to the honeycomb structure, the tetragonal lattice seems impossible according to the valence electron pair repulsion rule.[34] However, the planar tetracoordinated carbon has been first proposed by Hoffman *et al.* (1970)[35] and later synthesized in metal compound molecules (1977).[36] In organic chemistry, the compound having the shape of a square pyramid is called [3.3.3.3] fenestrane (or pyramidane), consisting of a central carbon atom which serves as a common vertex for four fused carbocycles. Experimentally, although this chemical compound has not been synthesized yet, the synthesis of related $Ge[C_4(SiMe_3)_4]$ and $Sn[C_4(SiMe_3)_4]$ has been reported.[37] Recent theoretical results also elaborate the existence of planar 4-coordinated C atoms in 2D materials, such as 2D BC compounds, t-TiC[38] and pentagraphene[39] *et al.* Thus, in consideration of the chemical similarity between carbon and silicon, it provides a possibility to produce a newly tetragonal silagraphene experimentally.

Herein, for the t-SiC monolayer, a possible strategy to obtain this sheet by hydrogen intercalation to break the subsurface C–Si covalent bonds in 3C–SiC is proposed. We first isolate the t-SiC sheet from the 3C–SiC substrate (the optimized structural model is shown in Fig. 6a) and check its structural stability by phonon calculation (Fig. 6b). Next, the effect of hydrogen intercalation in the subsurface of 3C–SiC for stripping a t-SiC monolayer is investigated by performing the AIMD simulation shown in Fig. 6c. After a period of time, the system reaches thermodynamic equilibrium, and a t-SiC monolayer with buckled structure is observed and stripped from the 3C–SiC film surface. Although this process may have high energy barriers, there is experimental evidence that hydrogen/deuterium can selectively interact with 3C–SiC substrate at the subsurface using high-resolution electron energy loss spectroscopy and synchrotron radiation-based photo-emission spectroscopy techniques.[40]

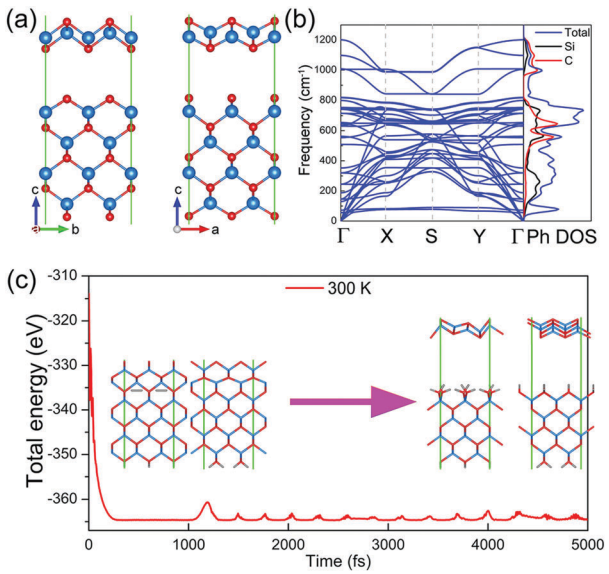


Fig. 6 (a) Structure of 3C–SiC (0001) surface containing the t-SiC monolayer and corresponding phonon spectrum (b). (c) The calculated energy evolution of hydrogen in intercalated 3C–SiC surface during AIMD simulation at 300 K. The insets show the initial and final structures viewed along the *a* and *b* directions, respectively.

## 4. Conclusions

In conclusion, we found two types of 2D SiC monolayers with unique bonding structures: tetragonal silagraphene and silagraphyne. The proposed tetragonal silagraphene sheets (t-SiC and t-$Si_2C$) exhibit a novel planar (quasi) tetracoordinated C–Si pattern, while the silagraphyne shows acetylenic linkages (sp carbon atoms) in the 2D crystal lattice. Then, kinetics and dynamics stability of the predicted monolayers were investigated by performing AIMD simulations and the calculations of phonon dispersion curves, respectively. Specifically, for the t-SiC monolayer, each Si atom is coordinated to four C atoms to form a tetragonal motif, which closely resembles pyramidane in structures with an approximate $D_{2h}$ symmetry. To our knowledge, such a monolayer purely consisting of quasi-planar covalent tetracoordinated carbon and silicon atoms has never been reported in the previous literature. Owing to its unique atomic patterns and strain-induced semiconductor to metal transition properties, t-SiC shows promise for applications in optoelectronic sensors when a suitable biaxial tensile strain is applied. Silagraphyne sheets have higher pore sizes, Poisson's ratio, and tunable band gap energies varying from 0.00 to 2.02 eV. These structural and electronic properties make silagraphyne as alternative materials for special applications that need softer materials and the next-generation photovoltaic devices. Finally, as a theoretical exploration, we propose a fabrication process using hydrogen intercalation to break the subsurface C–Si covalent bonds in 3C–SiC. In view of the distinct bonding structure and dynamics stability to endure the biaxial strain, these novel structures might be synthesized experimentally and used to fabricate photoelectric conversion devices with a high efficiency.

## Acknowledgements

This study was supported by the National Natural Science Foundation of China (Grant No. 50972129, 50602039, and 11504325), and Natural Science Foundation of Zhejiang Province (LQ15A040004). This study was also supported by the international science technology cooperation program of China (2014DFR51160).

## References

1 N. Narita, S. Nagai, S. Suzuki and K. Nakao, *Phys. Rev. B: Condens. Matter Mater. Phys.*, 1998, **58**, 11009.
2 K. Watanabe, T. Taniguchi and H. Kanda, *Nat. Mater.*, 2004, **3**, 404–409.
3 A. Pakdel, Y. Bando and D. Golberg, *Chem. Soc. Rev.*, 2014, **43**, 934–959.
4 P. He, H. Yu and H. Zhou, *J. Mater. Chem.*, 2012, **22**, 3680–3695.

 

5 H. Wang, H. Yuan, S. S. Hong, Y. Li and Y. Cui, *Chem. Soc. Rev.*, 2015, **44**, 2664–2680.
6 L. Li, Y. Yu, G. J. Ye, Q. Ge, X. Ou, H. Wu, D. Feng, X. H. Chen and Y. Zhang, *Nat. Nanotechnol.*, 2014, **9**, 372–377.
7 H. Şahin, S. Cahangirov, M. Topsakal, E. Bekaroglu, E. Akturk, R. T. Senger and S. Ciraci, *Phys. Rev. B: Condens. Matter Mater. Phys.*, 2009, **80**, 155453.
8 L. Tao, E. Cinquanta, D. Chiappe, C. Grazianetti, M. Fanciulli, M. Dubey, A. Molle and D. Akinwande, *Nat. Nanotechnol.*, 2015, **10**, 227–231.
9 S. Cahangirov, M. Topsakal, E. Aktürk, H. Şahin and S. Ciraci, *Phys. Rev. Lett.*, 2009, **102**, 236804.
10 F. Zhu, W. Chen, Y. Xu, C. Gao, D. Guan, C. Liu, D. Qian, S. C. Zhang and J. Jia, *Nat. Mater.*, 2015, **14**, 1020–1025.
11 X. Lin, S. Lin, Y. Xu, A. A. Hakro, T. Hasan, B. Zhang, B. Yu, J. Luo, E. Li and H. Chen, *J. Mater. Chem. C*, 2013, **1**, 2131–2135.
12 S. S. Lin, *J. Phys. Chem. C*, 2012, **116**, 3951–3955.
13 Y. Ding and Y. Wang, *J. Phys. Chem. C*, 2014, **118**, 4509–4515.
14 L. J. Zhou, Y. F. Zhang and L. M. Wu, *Nano Lett.*, 2013, **13**, 5431–5436.
15 Y. Li, F. Li, Z. Zhou and Z. Chen, *J. Am. Chem. Soc.*, 2011, **133**, 900–908.
16 Z. Shi, Z. Zhang, A. Kutana and B. I. Yakobson, *ACS Nano*, 2015, **9**, 9802–9809.
17 Y. Wang, J. Lv, L. Zhu and Y. Ma, *Phys. Rev. B: Condens. Matter Mater. Phys.*, 2010, **82**, 94116; Y. Wang, J. Lv, L. Zhu and Y. Ma, *Comput. Phys. Commun.*, 2012, **183**, 2063–2070; Y. Wang and Y. Ma, *J. Chem. Phys.*, 2014, **140**, 040901, http://www.calypso.cn.
18 S. Lu, Y. Wang, H. Liu, M. Miao and Y. Ma, *Nat. Commun.*, 2014, **5**, 3666.
19 X. Luo, J. Yang, H. Liu, X. Wu, Y. Wang, Y. Ma, S. H. Wei, X. Gong and H. Xiang, *J. Am. Chem. Soc.*, 2011, **133**, 16285–16290.
20 L. M. Yang, V. Bačić, I. A. Popov, A. I. Boldyrev, T. Heine, T. Frauenheim and E. Ganz, *J. Am. Chem. Soc.*, 2015, **137**, 2757–2762.
21 J. P. Perdew, K. Burke and M. Ernzerhof, *Phys. Rev. Lett.*, 1996, **77**, 3865.
22 G. Kresse and J. Furthmüller, *Phys. Rev. B: Condens. Matter Mater. Phys.*, 1996, **54**, 11169.
23 J. Heyd, G. E. Scuseria and M. Ernzerhof, *J. Chem. Phys.*, 2003, **118**, 8207–8215.
24 A. Togo and I. Tanaka, *Scr. Mater.*, 2015, **108**, 1–5.
25 A. R. Puigdollers, G. Alonso and P. Gamallo, *Carbon*, 2016, **96**, 879–887.
26 M. Xue, H. Qiu and W. Guo, *Nanotechnology*, 2013, **24**, 505720.
27 F. Fresno, R. Portela, S. Suárez and J. M. Coronado, *J. Mater. Chem. A*, 2014, **2**, 2863–2884.
28 Y. Li, L. Xu, H. Liu and Y. Li, *Chem. Soc. Rev.*, 2014, **43**, 2572–2586.
29 G. Li, Y. Li, H. Liu, Y. Guo, Y. Li and D. Zhu, *Chem. Commun.*, 2010, **46**, 3256–3258.
30 A. Molina-Sanchez and L. Wirtz, *Phys. Rev. B: Condens. Matter Mater. Phys.*, 2011, **84**, 155413.
31 R. C. Andrew, R. E. Mapasha, A. M. Ukpong and N. Chetty, *Phys. Rev. B: Condens. Matter Mater. Phys.*, 2012, **85**, 125428.
32 W. Shockley and H. J. Queisser, *J. Appl. Phys.*, 1961, **32**, 510–519.
33 Y. Guo, Q. Wang, Y. Kawazoe and P. Jena, *Sci. Rep.*, 2015, **5**, 14342.
34 W. L. Jolly, *Modern inorganic chemistry*, McGraw-Hill College, 1984.
35 R. Hoffmann, R. W. Alder and C. F. Wilcox Jr, *J. Am. Chem. Soc.*, 1970, **92**, 4992–4993.
36 F. A. Cotton and M. Millar, *J. Am. Chem. Soc.*, 1977, **99**, 7886–7891.
37 V. Y. Lee, Y. Ito, A. Sekiguchi, H. Gornitzka, O. A. Gapurenko, V. I. Minkin and R. M. Minyaev, *J. Am. Chem. Soc.*, 2013, **135**, 8794–8797.
38 Z. Zhang, X. Liu, B. I. Yakobson and W. Guo, *J. Am. Chem. Soc.*, 2012, **134**, 19326–19329.
39 S. Zhang, J. Zhou, Q. Wang, X. Chen, Y. Kawazoe and P. Jena, *Proc. Natl. Acad. Sci. U. S. A.*, 2015, **112**, 2372–2377.
40 P. Soukiassian, E. Wimmer, E. Celasco, C. Giallombardo, S. Bonanni, L. Vattuone, L. Savio, A. Tejeda, M. Silly and M. D'angelo, *Nat. Commun.*, 2013, **4**, 2800.
41 G. R. Berdiyorov and M. E. A. Madjet, *RSC Adv.*, 2016, **6**, 50867–50873.